Poly(amidoamine) Dendrimer as an Interfacial Dipole Modification in Crystalline Silicon Solar Cells

[1,2]*Thomas Tom*, [3]Eloi Ros*, [1,2]Julian López-Vidrier, [1,2]José Miguel Asensi, [3]Pablo Ortega,*

*[3]Joaquim Puigdollers, [1,2]Joan Bertomeu, [3]Cristobal Voz***

[1]Departament de Física Aplicada, Universitat de Barcelona (UB), Barcelona 08028, Spain [2]Institute of Nanoscience and Nanotechnology (IN^{2}UB), Barcelona 08028, Spain

[3]Departament d'Enginyeria Electrònica, Universitat Politècnica de Catalunya (UPC), Barcelona 08034, Spain

** Shared co-first authorship*
***Corresponding author*

ABSTRACT

Poly(amidoamine) (PAMAM) dendrimers are used to modify the interface of metal-semiconductor junctions. The large number of protonated amines contributes to the formation of a dipole layer, which finally serves to form electron selective contacts in silicon heterojunction solar cells. By modifying the work function of the contacts, the addition of the PAMAM dendrimer interlayer quenches Fermi level pinning, thus creating an ohmic contact between the metal and the semiconductor. This is supported by the observation of a low contact resistivity of 4.5 mΩ cm^2, the shift in work function, and the n-type behavior of PAMAM dendrimer films on the surface of crystalline silicon. A silicon heterojunction solar cell containing the PAMAM dendrimer interlayer is presented, which achieved a power conversion efficiency of 14.5%, an increase of 8.3% over the reference device without the dipole interlayer.

TOC GRAPHICS

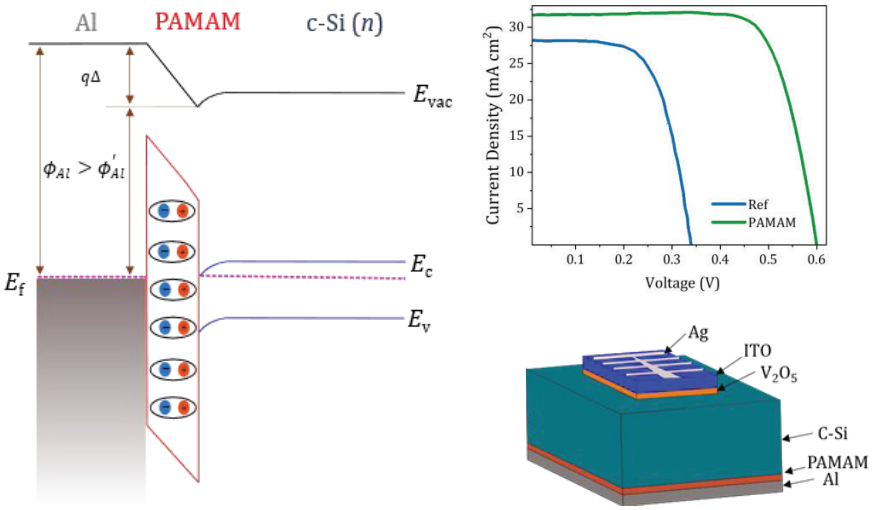

KEYWORDS - Fermi level pinning, Carrier selective contacts, Organic molecules, Conjugated polyelectrolytes, Vanadium pentoxide.

The development of carrier selective contacts in solar cells is of uttermost interest in the photovoltaics field, which seeks for the improvement of the power conversion efficiency (PCE) of heterojunction silicon solar cells[1,2]. In recent years, researchers have been trying to replace the heavily-doped hydrogenated amorphous silicon films that are used as carrier selective contacts, due to the complicated fabrication procedure they require, their parasitic absorption, and their high cost. With this objective in mind, various metal oxides, fluorides, nitrides and organic molecules have

been explored[3,4,5,6]. Amongst the latter, solution-processable organic semiconductor molecules have gained more acceptance due to their simple, low-cost, and low-temperature fabrication process, based on the spin coating technique.

Organic semiconductors are currently being widely investigated due to their specific features like low-production cost, limited processing time, light weight, and mechanical flexibility. They are utilized in visible lasers, light-emitting diodes, solar cells, and optical amplifiers[7,8,9,10]. Dendrimers are a new class of organic semiconductors that are well-defined multivalent non-dispersed macromolecules. Dendrimer show some advantages over other organic compounds due to better solubility determined by their functional groups, nano-scaled size and low viscosity[11,12,13,14]. Dendrimers have been studied in the past decade as an emerging material in photovoltaics. Mozer *et al.* investigated the charge transfer properties of different thiophene dendrimers in fullerene bulk heterojunction achieving a PCE of 0.72%[15]. Highly-efficient inverted-polymer solar cells with a solution-processable dendrimer as the electron-collection interlayer was investigated by V. Murugesan *et al.*, which yielded an efficiency of 3.53%[16]. The formation of an oriented dipole layer and the resulting Helmholtz potential have been cited as the origin of the conjugated polyelectrolytes working concept[17]. This potential allows for the modification of energy barriers that are often caused

by charge transfer events like Fermi level pinning at the interface between a semiconductor and a metal[18].

Here we report the electrical, optical, morphological, and dipolar characteristics of solution-processed thin films of poly(amidoamine) (PAMAM) generation zero (G0) dendrimer, whose 3D molecular structure is shown in Figure 1(a). As a proof of concept, the PAMAM dendrimer is used as an electron selective contact on dopant-free heterojunction solar cell with vanadium pentoxide (V_2O_5) as the hole selective contact, and therefore avoiding the use of expensive deposition systems to grow amorphous silicon layers. The solar cell fabricated using this configuration achieved a PCE of 14.5%, which supposes an 8.3% enhancement with respect to the reference device without the PAMAM dendrimer interlayer.

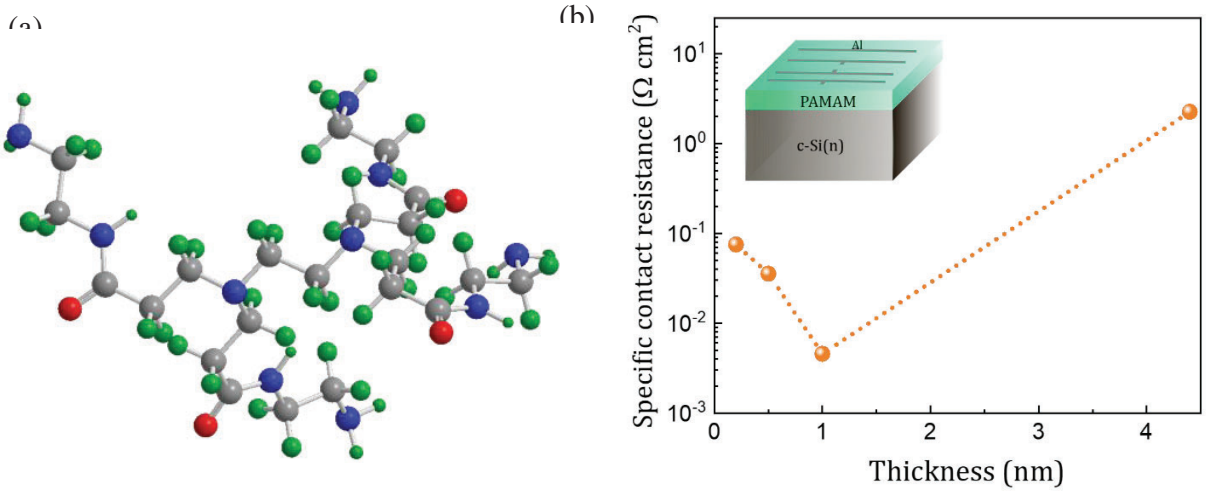

Figure 1. (a) 3D molecular structure of the PAMAM G0 dendrimer. Nitrogen (blue), Carbon (grey), Oxygen (red), Hydrogen (green). (b) The specific contact resistance for varying thickness of PAMAM dendrimer as extracted from the TLM measurements. The inset displays the TLM contact schematics for the measurements.

The current-voltage (*I–V)* characteristics of the PAMAM dendrimer films spin coated on *n*-type c-Si wafers were studied using the transfer length measurement (TLM) method. The thickness relationship with the contact resistance of the films is plotted in Figure 1(b). The inset shows the Al contact structure for TLM characterization. Different concentrations of the solution, from 0.001% to 0.1%, were used, the concentration as a function of thickness being shown in Figure S1 from the supplementary information. The optimum contact resistance, of 4.5 mΩ cm^2, was obtained for the 1-nm-thick film with 0.01% concentration. On the one hand, the contact becomes more resistive when increasing the film thickness, suggesting electron tunneling through the PAMAM dendrimer films as the dominating conduction mechanism. On the other hand, the increment in contact resistance below 1 nm indicates at least a secondary mechanism arising at close to monolayer thickness. Therefore, the optimum thickness of 1 nm, at a concentration of 0.1%, was chosen for the following studies.

The surface roughness of 1-nm-thick PAMAM dendrimer films on silicon substrates was studied by atomic force microscopy (AFM) and it is shown in Figure 2(a). The root mean square (RMS) roughness of the film is estimated to be 0.09 nm. The low surface roughness and lack of extended sharp peaks indicates a good uniformity of the PAMAM dendrimer films and enhanced wettability over the Si surface. Optical transmittance spectra were acquired from the same films (now deposited on sapphire substrates). The results corresponding to the 1-nm-thick sample (200–1500 nm range) are shown in Figure 2(b), exhibiting a high transmittance value over 95% throughout the spectrum. The inset shows the Tauc plot obtained from the transmittance data, with a calculated band gap of 4.7 eV. The high transparency and high optical band gap of the films contribute to their low absorption, making them more effective than traditional doped amorphous Si contacts.

The chemical analysis of the 1-nm-thick PAMAM dendrimer film on Si substrate was done using X-ray photoelectron spectroscopy (XPS). Figures. S2(a), (b), and (c) display the high-resolution C1s, N1s, and O1s XPS spectra (supplementary information). N1s spectra with peaks fitted at 398.7 and 401.1 eV can be attributed to amines and charged amine moieties. The charged amine moieties represent the positively charged N atoms in the PAMAM dendrimer films with protonated amines occupying 93% of the area in the spectrum[19,20,21,22,23]. This protonated amine group plays a major

role in charge transfer at the Al/PAMAM dendrimer/c-Si interface. It forms a dipole layer at the interface with protonated nitrogen as the positive and ethanolate from the counter ion condensation as the negative counterpart. This occurrence was proved in our previous work on polyethilimine[9].

The work function (WF) and valence band position of the film were obtained from UV photoelectron spectroscopy (UPS) measurements shown in Figure 2(c) and Figure S3 (supplementary information), respectively. The WF (ϕ) can be calculated using the relation, $\phi = h\nu - (E_{\text{cutoff}} - E_{\text{onset}}) - qV_{\text{bias}}$, where $h\nu$ is the incident UV photon energy (21.2 eV) and E_{cutoff} is the secondary-electron cutoff energy. The thin PAMAM dendrimer film lowers the WF from the reference *n*-type silicon (4.28 eV) down to 3.69 eV, in good accordance with the expected value[24,25]. This tuning of the apparent work function at the interface explains the formation of an ohmic contact and the resulting low specific contact resistivity. The work function shift ($q\Delta \approx 0.6\, eV$) also indicates the direction of the dipole formation with negative end pointing towards the electrode, and the positive end pointing towards the silicon substrate. The valence band edge of the c-Si (reference sample) is approximately 1 eV below the Fermi level, which is typical for *n*-type silicon. The PAMAM dendrimer film, on the other hand, has a valence band edge which is 2.81 eV lower than the Fermi level. We may then infer that the film shows an *n*-type character based on an optical band

gap of 4.7 eV and a valence band edge of 2.81 eV. Thus, the capability of the PAMAM dendrimer films to form the ohmic contact and the *n*-type character makes PAMAM dendrimer a promising candidate as electron selective contact in heterojunction solar cells.

(a)

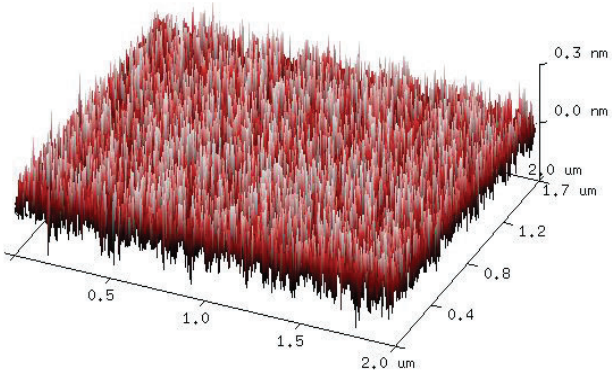
0.3 nm
0.0 nm
2.0 um
1.7 um
1.2
0.8
0.4
0.5
1.0
1.5
2.0 um

(b)

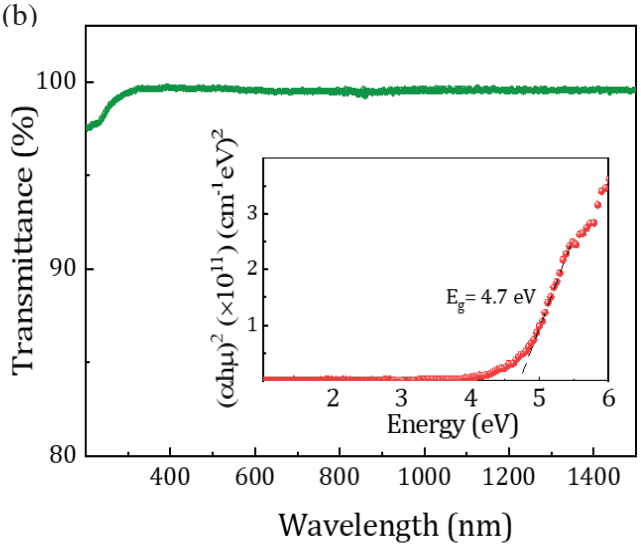
Transmittance (%)
100
90
80
400
600
800
1000
1200
1400
Wavelength (nm)
$(\alpha h\mu)^2$ $(\times 10^{11})$ $(cm^{-1}eV)^2$
3
2
1
E_g= 4.7 eV
2
3
4
5
6
Energy (eV)

(c)

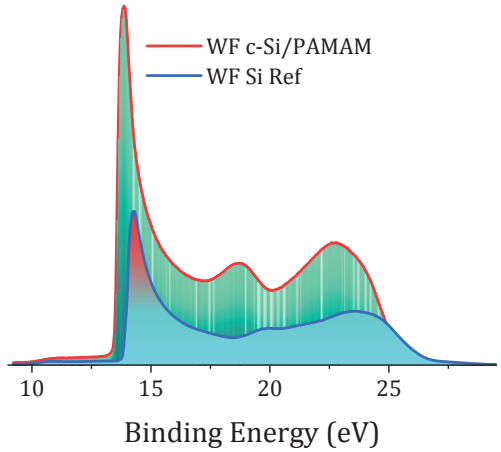
WF c-Si/PAMAM
WF Si Ref
10
15
20
25
Binding Energy (eV)

Figure 2. (a) AFM image of the 1-nm-thick PAMAM dendrimer film on c-Si (n) with RMS roughness of 0.09 nm. (b)Transmittance spectra of the same films on sapphire substrate, ranging from 200 nm to 1500 nm. The inset shows the corresponding Tauc plot, showing an optical band gap energy of 4.7 eV. (c) Analysis of the UPS spectra for the same films: work function. The UPS spectra corresponding to reference c-Si (n) sample are displayed for the sake of comparison.

The schematic representation of the energy band diagram with PAMAM dendrimer as the interlayer, proposed on the basis of the determined band gap energy, work function and valence band edge, is shown in Figure 3 (a). The PAMAM dendrimer forms a thin dipole intelayer due to the protonated amines, as observed from the XPS deconvolved spectra (Figure S2). In turn, this dipole formation between semiconductor and external electrode leads to the reduction of the apparent metal work function (ϕ'_{Al}) with respect to its non-altered value (ϕ_{Al}). Consequently, a significant charge transfer from Al to Si takes place that avoids Fermi level pinning at the surface.

Finally, as a proof of concept, a PAMAM dendrimer (1 nm)/Al selective electron contact was integrated into a 1×1 cm^2 doping-free heterojuntion silion solar cell. The V_2O_5 was the front hole selective contact and indium-doped tin oxide (ITO) layer as the transparent electrode. The schematic of the fabricated device is shown in the inset of Figure 3 (b), with an ITO/V_2O_5/c-Si/PAMAM dendrimer/Al structure. A reference device was also fabricated without the PAMAM dendrimer to show the superior performance of the solar cell incorporating a PAMAM dendrimer

dipole interlayer. Figure 3 (b) shows the current density-voltage (*J*–*V*) curves of both cells measured under 1 Sun illumination, and an overview of photovoltaic parameters of the solar cells is shown in Table 1. The evident increase of 260 mV in the open-circuit voltage (V_{oc}) of the PAMAM dendrimer-based solar cell compared to the reference device can be attributed to the reduced barrier energy at the interface due to the formation of an ohmic contact. Additionally, the elimination of Fermi level pinning and decrease of contact resistance contribute to increase the fill factor (*FF*). The PAMAM dendrimer-based solar cells have shown an enhanced *FF* over 76.2%, whereas the reference device exhibits a *FF* of only 64.4%. The 3.4 mA increase in short current density (J_{sc}) in PAMAM dendrimer cells could be probably attributed to electron accumulation at the interface and hence the improved surface passivation of silicon. Finally, the PAMAM dendrimer-based solar cells have shown a PCE of 14.5%, more than twice the performance of the reference device.

Table 1. Fill factor (*FF*), open-circuit voltage (V_{oc}), short-circuit current density (J_{sc}), and power conversion efficiency (PCE) of the fabricated solar cell, as well as the non-containing PAMAM dendrimer reference.

Table 1. Fill factor (*FF*), open-circuit voltage (V_{oc}), short-circuit current density (J_{sc}), and power conversion efficiency (PCE) of the fabricated solar cell, as well as the non-containing PAMAM dendrimer reference.

Structure of cells	***FF*** **(%)**	V_{oc} **(mV)**	J_{sc} **(mA cm^{-2})**	**PCE (%)**
ITO/V_2O_5/c-Si/Al (Ref)	64.4	339.8	28.3	6.2
ITO/V_2O_5/c-Si/PAMAM/Al	76.2	600.0	31.7	14.5

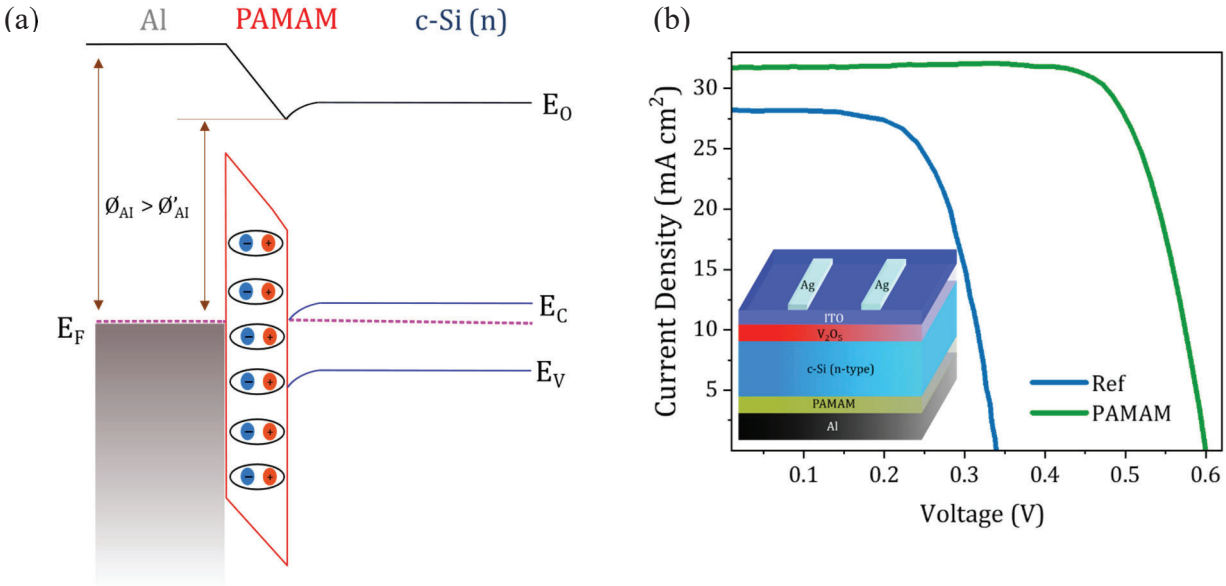

Figure 3. (a) Energy band diagram corresponding to the Si/PAMAM dendrimer/Al heterojunction. (b) *J–V* characteristics of the PAMAM dendrimer-based solar cell (in green) and the reference device without PAMAM dendrimer interlayer (in blue). The inset shows the architecture of the employed n-type silicon heterojunction cell integrated with a PAMAM dendrimer interlayer as electron selective contact.

In conclusion, the obtained results demonstrate that introducing the PAMAM dendrimer as a dipole interlayer between the semiconductor and the metal electrode improves the performance of the solar cell by lowering the metal work function and thereby suppressing the Fermi level pinning. As observed, the solar cell devices under study containing PAMAM dendrimer interlayer at the electron selective contact have doubled the efficiency with respect to the unmodified reference device. Ultimately, this work demonstrates the promising potential of dipole interlayers in optoelectronic devices whose performance (in this case due to photocarrier extraction) can be improved via interface and energy band engineering.

EXPERIMENTAL METHODS

PAMAM dendrimer of ethylenediamine core, generation 0.0 (G0), and dissolved in 20% methanol, with a linear formula $NH_2(CH_2)_2NH_2$, was purchased from Sigma Aldrich. Solutions containing different PAMAM dendrimer concentrations, from 0.1 to 0.001%, were prepared using methanol as the solvent. One-side polished (FZ) *n*-type c-Si (100) wafers (280 μm thickness, 2 Ω cm resistivity) and sapphire were used as substrates for various electrical and optical studies. Prior to deposition, all Si wafers were treated with 1% HF to achieve an oxide-free silicon surface.

PAMAM dendrimer was spin coated onto these substrates at 5000 rpm for 30 s and annealed in ambient air on a hot plate for 30 s at 90 ˚C. Thickness of the PAMAM dendrimer films was measured by ellipsometry, whereas spectroscopic measurements were done on samples deposited on sapphire glass substrates using UV-Visible-NIR spectrophotometer Lambda 950 (Perkin Elmer, Shelton, CT, USA). TLM were performed to investigate the specific contact resistance after thermally evaporating Al (300-nm-thick) contacts. Morphology studies were carried out using AFM on samples deposited on Si (Bruker Multimode 8 with Nanoscope, Santa Barbara, CA, USA). XPS and UPS measurements were performed using a Phoibos 150 analyzer (SPECS GmbH, Berlin, Germany). The peaks corresponding to N, C and O were deconvolved using the Casa XPS software. The work function was then estimated utilizing UPS data from the secondary electron cut-off. For the solar cell fabrication, a PAMAM dendrimer layer was spin coated onto a (non-texturized) one-side polished *n*-type silicon wafer followed by ambient-air annealing for 30 s. Afterwards, 300-nm-thick Al was thermally evaporated onto the films as the rear electrode. Atomic layer deposited (ALD) V_2O_5 was realized as the front hole selective contact followed by sputtering of 75-nm-thick ITO layer as the transparent electrode[19]. The active area of 1×1 cm^2 was defined using photolithography and Ag (1.5 μm) was thermally evaporated using a shadow mask as the

top grid. Using a 94041A solar simulator (Newport, Irvine, CA, USA), the *J–V* properties of the cells were tested under standard conditions of 100 mW/cm^2 and an AM1.5G spectrum. The external quantum efficiency analysis was conducted using the QEX10 configuration (PV Measurements, Point Roberts, WA, USA).

SUPPORTING INFORMATION

The Supporting Information is available as a separate document that includes:

- Figure S1. (a) Molecular structure of the PAMAM G0 dendrimer. (b) Thickness vs. concentration plot exhibiting a linear trend.
- Figure S2. (a)-(c) Deconvolved high-resolution XPS spectra of C1s (a), N1s (b), and O1s (c) bonds, for 1-nm-thick PAMAM dendrimer films on c-Si (n).
- Figure S3. Analysis of the UPS spectra of 1 nm films on silicon: valence band determination. The UPS spectra corresponding to reference c-Si (n) sample are displayed for the sake of comparison.
- Figure S4. External quantum efficiency of the PAMAM dendrimer-based solar cell.

AUTHOR INFORMATION

Corresponding Author

Cristobal Voz- Departament d'Enginyeria Electrònica, Universitat Politècnica de Catalunya (UPC), Barcelona 08034, Spain. Email: Cristobal.voz@upc.edu

Authors

Thomas Tom -Departament de Física Aplicada, Universitat de Barcelona (UB), Barcelona 08028, Spain and Institute of Nanoscience and Nanotechnology (IN2UB), Barcelona 08028, Spain. Email: thomastom@ub.edu

Eloi Ros- Departament d'Enginyeria Electrònica, Universitat Politècnica de Catalunya (UPC), Barcelona 08034, Spain. Email: eloi.ros@upc.edu

Julian López-Vidrier- Departament de Física Aplicada, Universitat de Barcelona (UB), Barcelona 08028, Spain and Institute of Nanoscience and Nanotechnology (IN2UB), Barcelona 08028, Spain. Email: jlopezv@ub.edu

José Miguel Asensi- Departament de Física Aplicada, Universitat de Barcelona (UB), Barcelona 08028, Spain and Institute of Nanoscience and Nanotechnology (IN2UB), Barcelona 08028, Spain. Email: jmasensi@ub.edu

Pablo Ortega- Departament d'Enginyeria Electrònica, Universitat Politècnica de Catalunya (UPC), Barcelona 08034, Spain. Email: pablo.rafael.ortega@upc.edu

Joaquim Puigdollers- Departament d'Enginyeria Electrònica, Universitat Politècnica de Catalunya (UPC), Barcelona 08034, Spain. Email: joaquim.puigdollers@upc.edu

Joan Bertomeu- Departament de Física Aplicada, Universitat de Barcelona (UB), Barcelona 08028, Spain and Institute of Nanoscience and Nanotechnology (IN2UB), Barcelona 08028, Spain.

Email: jbertomeu@ub.edu

Notes

The authors declare no conflict of interest.

ACKNOWLEDGMENTS

This research has been supported by the Spanish government through grants PID2019-109215RB-C41, PID2019-109215RB-C43, and PID2020-116719RB-C41 funded by MCIN/AEI/10.13039/501100011033. T. Tom acknowledges the support of the Secretaria d'Universitats i Recerca de la Generalitat de Catalunya and the European Social Fund (2019 FI_B 00456). In addition, the authors thank the technical staff from Barcelona Research Center in Multiscale Science and Engineering from the Universitat Politècnica de Catalunya for their expertise and helpful discussions over the XPS results, Dr. Oriol Arteaga from the Universitat de Barcelona for the ellipsometry measurements, and Guillaume Sauthier from the Catalan Institute

of Nanoscience and Nanotechnology for his contribution to UPS measurements and their discussion.

REFERENCES

(1) Wan, Y.; Samundsett, C.; Bullock, J.; Allen, T.; Hettick, M.; Yan, D.; Zheng, P.; Zhang, X.; Cui, J.; McKeon, J.; Javey, A.; Cuevas, A. Magnesium Fluoride Electron-Selective Contacts for Crystalline Silicon Solar Cells. *ACS Appl Mater Interfaces* **2016**, *8* (23), 14671–14677. https://doi.org/10.1021/acsami.6b03599.

(2) Gao, P.; Yang, Z.; He, J.; Yu, J.; Liu, P.; Zhu, J.; Ge, Z.; Ye, J. Dopant-Free and Carrier-Selective Heterocontacts for Silicon Solar Cells: Recent Advances and Perspectives. *Advanced Science* **2017**, 1700547. https://doi.org/10.1002/advs.201700547.

(3) Wan, L.; Zhang, C.; Ge, K.; Yang, X.; Li, F.; Yan, W.; Xu, Z.; Yang, L.; Xu, Y.; Song, D.; Chen, J. Conductive Hole-Selective Passivating Contacts for Crystalline Silicon Solar Cells. *Adv Energy Mater* **2020**, *10* (16), 1–8. https://doi.org/10.1002/aenm.201903851.

(4) Battaglia, C.; de Nicolás, S. M.; De Wolf, S.; Yin, X.; Zheng, M.; Ballif, C.; Javey, A. Silicon Heterojunction Solar Cell with Passivated Hole Selective MoO x Contact. *Appl Phys Lett* **2014**, *104* (11), 113902. https://doi.org/10.1063/1.4868880.

(5) Yu, J.; Yu, J.; Yu, J.; Phang, P.; Samundsett, C.; Basnet, R.; Neupan, G. P.; Yang, X.; Macdonald, D. H.; Wan, Y.; Yan, D.; Ye, J. Titanium Nitride Electron-Conductive Contact for Silicon Solar Cells by Radio Frequency Sputtering from a TiN Target. *ACS Appl Mater Interfaces* **2020**, *12* (23), 26177–26183. https://doi.org/10.1021/ACSAMI.0C04439/SUPPL_FILE/AM0C04439_SI_001.PDF.

(6) Yang, Z.; Gao, P.; He, J.; Chen, W.; Yin, W. Y.; Zeng, Y.; Guo, W.; Ye, J.; Cui, Y. Tuning of the Contact Properties for High- Efficiency Si/PEDOT:PSS Heterojunction Solar Cells. *ACS Energy Lett* **2017**, *2* (3), 556–562. https://doi.org/10.1021/acsenergylett.7b00015.

(7) Kunkel, C.; Margraf, J. T.; Chen, K.; Oberhofer, H.; Reuter, K. Active Discovery of Organic Semiconductors. *Nat Commun* **2021**, *12* (1), 1–11. https://doi.org/10.1038/s41467-021-22611-4.

(8) Giannini, S.; Blumberger, J. Charge Transport in Organic Semiconductors: The Perspective from Nonadiabatic Molecular Dynamics. *Acc Chem Res* **2022**, *55* (6), 819–830. https://doi.org/10.1021/acs.accounts.1c00675.

(9) Ros, E.; Tom, T.; Rovira, D.; Lopez, J.; Masmitjà, G.; Pusay, B.; Almache, E.; Martin, I.; Jimenez, M.; Saucedo, E.; Tormos, E.; Asensi, J. M.; Ortega, P.; Bertomeu, J.; Puigdollers, J.; Voz, C. Expanding the Perspective of Polymeric Selective Contacts in Photovoltaic Devices Using Branched Polyethylenimine. *ACS Appl Energy Mater* **2022**, *5* (9), 10702–10709. https://doi.org/10.1021/acsaem.2c01422.

(10) Bronstein, H.; Nielsen, C. B.; Schroeder, B. C.; McCulloch, I. The Role of Chemical Design in the Performance of Organic Semiconductors. *Nat Rev Chem* **2020**, *4* (2), 66–77. https://doi.org/10.1038/s41570-019-0152-9.

(11) Burroughes, J. H.; Bradley, D. D. C.; Brown, A. R.; Marks, R. N.; Mackay, K.; Friend, R. H.; Burns, P. L.; Holmes, A. B. Light-Emitting Diodes Based on Conjugated Polymers. *Nature* **1990**, *347* (6293), 539–541. https://doi.org/10.1038/347539a0.

(12) Zeng, Y.; Li, Y. Y.; Chen, J.; Yang, G.; Li, Y. Dendrimers: A Mimic Natural Light-Harvesting System. *Chem Asian J* **2010**, *5* (5), 992–1005. https://doi.org/10.1002/asia.200900653.

(13) Abbasi, E.; Aval, S. F.; Akbarzadeh, A.; Milani, M.; Nasrabadi, H. T.; Joo, S. W.; Hanifehpour, Y.; Nejati-Koshki, K.; Pashaei-Asl, R. Dendrimers: Synthesis, Applications, and Properties. *Nanoscale Res Lett* **2014**, *9* (1), 247. https://doi.org/10.1186/1556-276X-9-247.

(14) Kim, K. H.; Chi, Z.; Cho, M. J.; Choi, D. H.; Kang, H. S.; Cho, M. Y.; Joo, J. S. P-Type Semiconducting Dendrimers Bearing Thiophenyl Peripheral Moieties for Organic Field Effect Transistors. *Appl Phys Lett* **2006**, *89* (20). https://doi.org/10.1063/1.2388244.

(15) Mozer, A. J.; Ma, C. Q.; Wong, W. W. H.; Jones, D. J.; Bäuerle, P.; Wallace, G. G. The Effect of Molecule Size and Shape on Free Charge Generation, Transport and Recombination in All-Thiophene Dendrimer:Fullerene Bulk Heterojunctions. *Org Electron* **2010**, *11* (4), 573–582. https://doi.org/10.1016/j.orgel.2009.12.016.

(16) Murugesan, V.; Sun, K.; Ouyang, J. Highly Efficient Inverted Polymer Solar Cells with a Solution-Processable Dendrimer as the Electron-Collection Interlayer. *Appl Phys Lett* **2013**, *102* (8). https://doi.org/10.1063/1.4794065.

(17) Liu, P. H.; Chuang, C. H.; Zhou, Y. L.; Wang, S. H.; Jeng, R. J.; Rwei, S. P.; Liau, W. Bin; Wang, L. Conjugated Polyelectrolytes as Promising Hole Transport Materials for Inverted Perovskite Solar Cells: Effect of Ionic Groups. *J Mater Chem A Mater* **2020**, *8* (47), 25173–25177. https://doi.org/10.1039/d0ta09063h.

(18) Zhang, Z.; Yates, J. T. Band Bending in Semiconductors: Chemical and Physical Consequences at Surfaces and Interfaces. *Chem Rev* **2012**, *112* (10), 5520–5551. https://doi.org/10.1021/cr3000626.

(19) Tom, T.; Ros, E.; López-Pintó, N.; Asensi, J. M.; Andreu, J.; Bertomeu, J.; Puigdollers, J.; Voz, C. Influence of Co-Sputtered Ag:Al Ultra-Thin Layers in Transparent V2O5/Ag:Al/AZO Hole-Selective Electrodes for Silicon Solar Cells. *Materials 2020, Vol. 13, Page 4905* **2020**, *13* (21), 4905. https://doi.org/10.3390/MA13214905.

(20) Karakoçak, B. B.; Liang, J.; Kavadiya, S.; Berezin, M. Y.; Biswas, P.; Ravi, N. Optimizing the Synthesis of Red-Emissive Nitrogen-Doped Carbon Dots for Use in Bioimaging. *ACS Appl Nano Mater* **2018**, *1* (7), 3682–3692. https://doi.org/10.1021/acsanm.8b00799.

(21) Viltres, H.; Odio, O. F.; Biesinger, M. C.; Montiel, G.; Borja, R.; Reguera, E. Preparation of Amine- and Disulfide-Containing PAMAM-Based Dendrons for the Functionalization of Hydroxylated Surfaces: XPS as Structural Sensor. *ChemistrySelect* **2020**, *5* (16), 4875–4884. https://doi.org/10.1002/slct.202000432.

(22) Demirci, S.; Emre, F. B.; Ekiz, F.; Oguzkaya, F.; Timur, S.; Tanyeli, C.; Toppare, L. Functionalization of Poly-SNS-Anchored Carboxylic Acid with Lys and PAMAM: Surface Modifications for Biomolecule Immobilization/Stabilization and Bio-Sensing Applications. *Analyst* **2012**, *137* (18), 4254–4261. https://doi.org/10.1039/c2an35472a.

(23) Tom, T.; Ros, E.; Rovira, D.; López-Vidrier, J.; Asensi, J. M.; Ortega, P.; Puigdollers, J.; Voz, C.; Bertomeu, J. Deoxyribonucleic Acid-Based Electron Selective Contact for Crystalline Silicon Solar Cells. *Adv Mater Technol* **2022**, 2200936. https://doi.org/10.1002/ADMT.202200936.

(24) Ji, W.; Allen, T.; Yang, X.; Zeng, G.; De Wolf, S.; Javey, A. Polymeric Electron-Selective Contact for Crystalline Silicon Solar Cells with an Efficiency Exceeding 19%. *ACS Energy Lett* **2020**, *5* (3), 897–902. https://doi.org/10.1021/ACSENERGYLETT.0C00110/SUPPL_FILE/NZ0C00110_SI_001.PDF.

(25) Menzel, D.; Mews, M.; Rech, B.; Korte, L. Electronic Structure of Indium-Tungsten-Oxide Alloys and Their Energy Band Alignment at the Heterojunction to Crystalline Silicon. *Appl Phys Lett* **2018**, *112* (1). https://doi.org/10.1063/1.5010278.